Cooperative differentiation through clustering in multicellular populations

A. Koseska, E. Ullner, E. Volkov, J. Kurths, J. García-Ojalvo

Cooperative differentiation through clustering in multicellular populations

A. Koseska, E. Ullner, E. Volkov, J. Kurths, J. García-Ojalvo

PII: S0022-5193(09)00533-5
DOI: doi:10.1016/j.jtbi.2009.11.007
Reference: YJTBI 5772

To appear in: *Journal of Theoretical Biology*

Received date: 10 July 2009
Revised date: 23 October 2009
Accepted date: 10 November 2009

Cite this article as: A. Koseska, E. Ullner, E. Volkov, J. Kurths and J. García-Ojalvo, Cooperative differentiation through clustering in multicellular populations, *Journal of Theoretical Biology*, doi:10.1016/j.jtbi.2009.11.007

Cooperative differentiation through clustering in multicellular populations

A. Koseska[*,a], E. Ullner[b,c,d,e], E. Volkov[f], J. Kurths[g,h], J. García-Ojalvo[d]

[a] *Center for Dynamics of Complex Systems, University of Potsdam, D-14469 Germany*
[b] *Institute for Complex Systems and Mathematical Biology, King College, University of Aberdeen, Aberdeen AB24 3UE, United Kingdom*
[c] *Institute of Medical Sciences, Forresterhill, University of Aberdeen, Aberdeen AB25 2DZ, United Kingdom*
[d] *Departament de Física i Enginyeria Nuclear, Universitat Politècnica de Catalunya, Colom 11, E-08222 Terrassa, Spain*
[e] *Institute for Theoretical Biology (ITB), Humboldt University, Invalidenstr. 43, D-10115 Berlin, Germany*
[f] *Department of Theoretical Physics, Lebedev Physical Inst., Leninskii 53, Moscow, Russia*
[g] *Institute of Physics, Humboldt University Berlin, D-10099 Germany*
[h] *Potsdam Institute for Climate Impact Research, D-14412 Germany*

Abstract

The coordinated development of multicellular organisms is driven by intercellular communication. Differentiation into diverse cell types is usually associated with the existence of distinct attractors of gene regulatory networks, but how these attractors emerge from cell-cell coupling is still an open question. In order to understand and characterize the mechanisms through which coexisting attractors arise in multicellular systems, here we systematically investigate the dynamical behavior of a population of synthetic genetic oscillators coupled by chemical means. Using bifurcation analysis and numer-

[*] Corresponding author
Email addresses: koseska@yahoo.com (A. Koseska), e.ullner@abdn.ac.uk (E. Ullner), volkov@td.lpi.ru (E. Volkov), kurths@pik-potsdam.de (J. Kurths), jordi.g.ojalvo@upc.edu (J. García-Ojalvo)

ical simulations, we identify various attractors and attempt to deduce from these findings a way to predict the organized collective behavior of growing populations. Our results show that dynamical clustering is a generic property of multicellular systems. We argue that such clustering might provide a basis for functional differentiation and variability in biological systems.

Key words:

Multicellular systems, clustering, collective behavior, inhibitory cell-to-cell communication, cellular differentiation

1. Introduction

The coordinated behavior in multicellular systems results from a cooperative response arising from an integrated exchange of information through cell-cell communication. Various mechanisms for intercellular coupling have been identified in nature, basically relying on the broadcasting of individual cellular states to neighboring cells via intercellular signals, which are further integrated to generate a global system's response (Heinlein (2002); Perbal (2003)). It is known, for instance, that bacteria display various types of collective behavior driven by a type of chemical cell-cell communication mechanism known as quorum sensing (Taga and Bassler (2003)). This ability of living systems is an absolute requisite to ensure an appropriate and robust global cellular response of an organism in a noisy environment. Hence, characterizing the dynamics of multicellular systems should lead to an improvement of our knowledge about cellular behavior and biological mechanisms that occur on a population-wide scale, such as cellular differentiation, adaptability of the system to different environment conditions, etc.

In order to understand the basic mechanisms of cell-to-cell cooperative behavior, several theoretical models have been successfully developed and investigated by studying both natural and synthetic genetic networks (McMillen et al. (2002); Taga and Bassler (2003); Kuznetsov et al. (2004); García-Ojalvo et al. (2004); Ullner et al. (2007); Balagadde et al. (2008); Tanouchi et al. (2008)). A synchronization scheme has been proposed, for instance, in an artificial network of synthetic genetic oscillators that produces and responds to a specific, small signaling molecule (acylated homoserine lactone), known as an autoinducer (AI) (García-Ojalvo et al. (2004)). This small molecule is

free to diffuse through the cell membrane, which provides a means for chemical communication between neighboring cells. The resulting synchronized behavior leads to a macroscopic genetic clock. By further manipulations of this synthetic network, we were able to show (Ullner et al. (2007, 2008)) that this communication scheme can be re-engineered to produce a very diverse dynamics and exhibit a high adaptability typical to natural systems. Other modification of the same network (García-Ojalvo et al. (2004)) was also published recently (Zhou et al. (2008)), but it still waits futher dynamical investigations.

In this paper, we investigate systematically the global cooperative behavior of a population of synthetic genetic oscillators called repressilators, coupled via quorum sensing mechanism (Ullner et al. (2007)), and thus showing the emergence of a rich variety of clustering behavior that might be interpreted as a mechanism of dynamical differentiation. Such an interpretation was pioneered by Turing (Turing (1952)) in his investigations of inhomogeneous steady states in reaction-diffusion systems, and has been further extended by Kaneko (Kaneko and Yomo (1994)), who proposed clustering in coupled map dynamics as a physical background of biological differentiation. Moreover, it was recently shown (Nakajima and Kaneko (2008)) that bifurcations driven by cell-cell interaction may mediate differentiation processes.

Here we use numerical simulations and bifurcation analysis to study the dynamics of a population of coupled genetic oscillators for increasing sizes of the population, ranging from a two-cell to a multicellular system, thus proposing a general explanation for the emergence of cooperative behavior in large cellular systems. In our previous work (Ullner et al. (2007, 2008))

we investigated and defined the necessary coupling conditions leading to a complex dynamical behavior in the system, and furthermore clasified its dynamical structure using a minimal system of $N = 2$ oscillators. In addition to those earlier results, here we show that the extended system exhibits various attractors with complex phase relations, and through their characterization we attempt to (i) deduce the underlying mechanism that determines the most likely visited dynamical regimes, and (ii) identify stable cluster distributions, in order to predict the behavior of the system on a global scale. The bifurcation analysis and numerical investigations presented here also aim to characterize the robustness of the dynamical structure of the system with respect to parameter variations, and relate these findings to biological processes. We stress here the importance of investigating dynamical clustering in multicellular populations with cell-cell communication, since such coupling generates qualitatively new cellular states different from the single-cell dynamics, thus providing the basis for functional differentiation and variability.

Moreover, in (Ullner et al. (2008)) we identified a biologically relevant parameter interval where chaotic behavior of the coupled genetic units was observed. As previously suggested, this could implicate chaos as an additional source of uncertainty in gene expression, drawing attention on possible alternative sources of uncertainty in genetic networks, besides the already well-established ones. It is therefore important to investigate the dynamical behavior of cell populations in the chaotic regime, and identify possible groupings of genetic oscillators and their relations within, as a base for envisioning an experimental protocol to detect chaotic behavior in synthetic genetic networks.

2. Model of a synthetic multicellular system

The model considered here consists of a population of repressilators coupled via quorum-sensing mechanism as proposed in (Ullner et al. (2007)). The repressilator consists of three genes whose protein products repress the transcription of each other in a cyclic way (Elowitz and Leibler (2000)). In its original experimental implementation, the gene *lacI* expresses protein $LacI$, which inhibits transcription of the gene *tetR*. The product of the latter, $TetR$, inhibits transcription of the gene *cI*. Finally, the protein product CI of the gene *cI* inhibits expression of *lacI* and completes the cycle (see Fig. 1). An additional feedback loop involving the two proteins $LuxI$ and $LuxR$, which might be placed on a separate plasmid, realizes the cell-to-cell communication (McMillen et al. (2002); You et al. (2004); García-Ojalvo et al. (2004)). $LuxI$ is responsible for the biosynthesis of a small signaling molecule, known as autoinducer (AI), which diffuses through the cell membrane and thus provides a means of intercellular communication. By forming a stable $AI - LuxR$ complex, the transcription of a second copy of the repressilator gene *lacI* is activated. Placing the gene *luxI* under inhibitory control of the repressilator protein $TetR$ (Fig. 1) introduces a rewiring between the repressilator and the quorum sensing through an additional loop, which competes with the overall negative feedback loop along the repressilator ring and results in an inhibitory, phase-repulsive intercellular coupling.

The $mRNA$ dynamics is described by the following Hill-type kinetics with Hill coefficient n:

$$\dot{a}_i = -a_i + \frac{\alpha}{1 + C_i^n} \tag{1}$$

$$\dot{b}_i = -b_i + \frac{\alpha}{1 + A_i^n} \quad (2)$$

$$\dot{c}_i = -c_i + \frac{\alpha}{1 + B_i^n} + \kappa \frac{S_i}{1 + S_i} \quad (3)$$

where the subindex i denotes the cell ($i = 1, .., N$, N being the total number of cells in the ensemble), and a_i, b_i and c_i represent the concentrations of $mRNA$ molecules transcribed from *tetR*, *cI* and *lacI*, respectively. The model is made dimensionless by measuring time in units of the $mRNA$ lifetime (assumed equal for all genes) and the $mRNA$ and protein levels in units of their Michaelis constants (assumed equal for all genes). The $mRNA$ concentrations are additionally rescaled by the ratio of their protein degradation (different among the genes) and translation rates (assumed equal for all genes). After rescaling, α is the dimensionless transcription rate in the absence of a repressor, κ is the maximum transcription rate of the $LuxR$ promoter, and the parameters $\beta_{a,b,c}$ describe the ratios between the $mRNA$ and protein lifetimes (inverse degradation rates). We assume different lifetime ratios for the protein/$mRNA$ pairs, which results in a weak relaxator-like dynamics of the repressilator (Ullner et al. (2007)). A_i, B_i, and C_i denote the concentration of the proteins *TetR*, *CI*, and *LacI*, whose dynamical behavior is given by:

$$\dot{A}_i = \beta_a(a_i - A_i) \quad (4)$$

$$\dot{B}_i = \beta_b(b_i - B_i) \quad (5)$$

$$\dot{C}_i = \beta_c(c_i - C_i) \quad (6)$$

Assuming equal lifetimes and dynamics for both the CI and $LuxI$ proteins (since they are both repressed by TetR), we use the same variable to

describe the dynamics of both proteins. The AI concentration S_i in the $i-th$ cell (rescaled additionally by its Michaelis constant) is proportional to B_i, i.e. the concentration of $LuxI$ in it, and is further affected by an intracellular degradation and diffusion toward or from the intercellular space:

$$\dot{S}_i = -k_{s0}S_i + k_{s1}B_i - \eta(S_i - S_e) \quad (7)$$

$$S_e = Q\bar{S} \quad (8)$$

$$\bar{S} = \frac{1}{N}\sum_{i=1}^{N} S_i \quad (9)$$

The diffusion coefficient η depends on the permeability of the membrane to the autoinducer. Due to the fast diffusion of the extracellular AI (S_e) compared to the repressilator period, we can apply the quasi-steady-state approximation to the dynamics of the external AI and replace it by the mean field of the internal AI, $\bar{S}$. The parameter Q is defined as $Q = \frac{\delta N/V_{ext}}{k_{se}+\delta N/V_{ext}}$ (García-Ojalvo et al. (2004)), with N being the total number of cells in the ensemble, V_{ext} the total extracellular volume, k_{se} the extracellular AI degradation rate, and δ the product of the membrane permeability and the surface area. In more general terms, Q is proportional to the cell density, and can be varied in a controlled way between 0 and 1 in experiment, thus making it a reasonable choice to follow the dynamical changes of the system with respect to Q.

Previous investigations carried on a minimal system of two repressilators coupled via repulsive cell-to-cell communication (Ullner et al. (2008)) have identified a variety of collective regimes, including constant level protein production (homogeneous steady state solution, HSS, Fig. 2a), an inhomogeneous steady state characterized by different stationary protein levels (IHSS,

Fig. 2b), and self-sustained oscillations. Within the latter case, we have identified out-of-phase oscillations with different phase shifts (see e.g. Fig. 2c, for which the phase shift is $\frac{\pi}{2}$), as well as a complex inhomogeneous limit cycle (IHLC) characterized by one cell exhibiting very small oscillations around a high mean protein level, whereas the second cell oscillates in the vicinity of the steady state with an amplitude just slightly smaller than that of an isolated oscillator (Fig. 2d).

The previous results correspond to a fixed value $N = 2$. However, *in vivo* bacterial colonies proliferate and expand. In order to understand and characterize the cooperative behavior in growing populations, it is certainly of outmost significance to investigate the influence of the size of the population on its dynamics. To that end, we performed a simple numerical experiment: we computed 1000 time series with different random initial conditions for a minimal ($N = 2$ cells), and a system with intermediate size ($N = 18$), using a uniform distribution in the range $[0, 220]$ for the $mRNA$ and protein initial conditions and $[0, 1.2]$ for the AI initial conditions. Figure 3 shows the histograms of detectable stable regimes in both systems for increasing coupling coefficient Q.

As shown in Fig. 3, already a small increase in the system size (from $N = 2$ to $N = 18$ cells) alters the balance between the coexisting regimes: the stability regions of IHLC and IHSS are significantly increased at the expense of the HSS. This fact underlines the connection between the size of the population and its dynamical behavior, implying that a detailed analysis of these correlations is necessary in order to reveal and formulate (predict) a general statement about the cooperative behavior of growing populations.

3. Clustering in the inhomogeneous regimes

It is well known that genetically identical cells may exhibit diverse phenotypic states even under almost identical environmental conditions. Thus, populations comprised of identical cellular units can display heterogeneity, manifested by the existence of several subgroups or clusters where cells exhibit organized collective behavior, with or without complex relations among them. The size of the population plays a crucial role in determining which dynamical behavior is most likely to be dominant, depending of course on the environmental conditions as well as on the coupling strengths.

We now show that the parameter stability intervals for given solutions increase significantly as a function of N, with respect to the equivalent stability intervals in the minimal model of two coupled cells (Ullner et al. (2008)). These changes in the dynamical structure of the model occur in general due to the increased possibility for cluster formation in growing populations. Clustering can be defined as a stable dynamical state characterized by the coexistence of several subgroups where the oscillators exhibit identical (or nearly identical) behavior. Clustering is a well known property, especially for globally coupled systems, and has been investigated for identical phase (Golomb et al. (1992); Okuda (1993)), salt-water (Miyakawa and Yamada (2001)) or electrochemical oscillators (Wang et al. (2001); Kiss and Hudson (2003)), in synthetic genetic networks (Koseska et al. (2007)), and in populations of chaotic oscillators (Kuznetsov and Kurths (2002); Manruiba and Mikhailov (1999); Osipov et al. (2007)), among other cases. The presence of clustering and the complex phase relations between cells produced therewith can be very important in the construction of synthetic genetic networks and

the mechanisms behind cell differentiation. Therefore, our attention will be mainly devoted to clustering that occurs in the inhomogeneous states (steady or oscillatory), and which could be related to biological mechanisms of dynamical differentiation. Moreover, different groupings that occur mainly in the chaotic regime and contribute significantly to the complex dynamical behavior on a population-wide scale will be also of significant interest to us. This is because such groupings can be also seen as a mechanism for temporal mixing that enhances the diversity in the system, while mostly maintaining the advantages of a synchronized (ordered collective) behavior.

As a first step, a minimal extension to $N = 3$ identical cells was introduced, in order to classify the dynamical changes leading to clustering. We now present bifurcation diagrams for that case, with the coupling strength Q as the bifurcation parameter. As discussed above, Q is proportional to the extracellular cell density and can be changed experimentally in chemostat experiments in the range between zero and one. Values beyond this range do not have a biological meaning but can be helpful for the understanding of the bifurcation analysis and the controlling of desired regimes. Although the complete bifurcation analysis was performed using the *Xppaut* package (Ermentrout (2002)), the diagrams presented here depict only those bifurcation branches and points central to the corresponding discussion, in order to avoid making the bifurcation charts incomprehensible.

The bifurcation analysis revealed a significant enlargement of the stability interval for the $IHSS$ ($Q \in [0.29 - 0.66]$, Fig. 4(b)), in comparison to the minimal case of $N = 2$ coupled oscillators ($Q \in [0.36 - 0.55]$) (Fig. 4(a) and in (Ullner et al. (2008))). The $IHSS$ is stabilized via a Hopf bifurcation, thus

displaying no qualitative changes in the mechanism of occurrence with respect to the minimal model. However, the significant increase of the stability region in this case ($\approx 50\%$ in comparison to $N = 2$) is a result of clustering, or more specifically, of the increased number of possible distributions of the oscillators between the two stable protein levels through which the $IHSS$ is defined. In general, given N total number of cells, the oscillators can have $N-1$ different distributions between the clusters (considering that the $IHSS$, as well as the $IHLC$ discussed below, are characterized by two-cluster decompositions). In what follows, we will define the different cluster states by the notation $mL \mid (N-m)U$, which denotes a cluster of m oscillators in the low-protein concentration state L, while the remaining $N-m$ oscillators populate the upper state U, characterized by higher protein concentration. For $N = 2$ cells, there is only one possible distribution of the oscillators in the $IHSS$ regime: $1L \mid 1U$ - one oscillator populates the lower, where the second one populates the upper state. However, for an increased number of cells, $N = 3$, there are 2 different combinations, namely $1L \mid 2U$ (Fig. 4b, left stable branch (solid (green) line)) and $2L \mid 1U$ (Fig. 4b, right stable branch (solid (green) line)). Note that different stable cluster distributions are located on separate branches of the bifurcation continuation, thus resulting in the increase of the parameter interval where IHSS exists. In the case of $N = 5$ oscillators, for example, 4 different clusters are stable, as shown in Fig. 4(c). In that diagram the cluster types are, from left to right: $1L \mid 4U$, $2L \mid 3U$, $3L \mid 2U$ and $4L \mid 1U$. This particular structure of cluster distribution is typical for any number of oscillators: clusters of the type $1L \mid (N-1)U$ require small Q values, while the $(N-1)L \mid 1U$ exist for large Q. In order to understand this

behavior, let us define the ratio of the oscillators distributed in the upper versus lower B_i states as $r = \frac{N-m}{m}$. Suppose that under small Q, r is larger than one ($r > 1$ means that the majority of the oscillators in the system are located in the upper B state). Let us know assume that the value of r decreases, until $r < 1$. This means that the total concentration of the protein CI (B) in the system is decreased. Moreover, since the dynamics of the AI follows closely the dynamics of the protein B (both expressions, that of protein B (cI) and of AI ($luxI$) are regulated in a same manner via $tetR$), the production of internal AI will also be decreased. In order to compensate for the lack of internal AI which will destabilze the $IHSS$, the re-influx of external AI needs to be increased. This will subsequently lead to higher Q values which means that in general, if $r < 1$, larger Q is necessary to observe stable $IHSS$ distributions.

The left and middle plots in Fig. 5 show time traces for two different cluster decomposition in the $IHSS$ regime for $N = 18$. Each possible partition shows slightly different levels in the protein concentrations, and hence a fine tuning of the protein levels can be accomplished by choosing a specific Q interval for proper partition of the oscillators. This specific effect enhances, on the one hand, the biotechnological applications of synthetic genetic networks by providing a possible method for fine manipulation of the protein concentration level, and on the other hand it might be seen as typical adaptability of a cell population: when changes in the environmental conditions occur, the population can easily adjust its cell distribution, adapting optimally to the environment.

The Hopf bifurcation through which the $IHSS$ is stabilized gives rise also

to a branch of stable inhomogeneous limit cycles ($IHLC$), already introduced for the case of $N = 2$ oscillators in Fig. 2(d) (the corresponding bifurcation diagram is given in Fig. 6(a)). However, in comparison to that minimal case, the $IHLC$ regime for higher population sizes is more complex, due to the increased number of possibilities for distributing the oscillators in the two clusters (a stable and an oscillating one).

Analogous to the formation of $IHSS$ clusters for $N = 3$, two distinct $IHLC$ clusters can be observed here as well. We have identified these regimes as $1L \mid 2U$ (left solid (red) line in Fig. 6, (b)), and $2L \mid 1U$ (right solid (red) line in Fig. 6 (b)), emerging from the correspondent $IHSS$ branches (Hopf bifurcations of the $IHSS$, HB_{s1} and HB_{s2} in Figs. 4(b), 6(b)). This results again in an interval where the $IHLC$ regime is stable in comparison to the 2-oscillator case (compare Figs. 6 (a) and (b)). Moreover, the $IHSS$ and $IHLC$ regimes coexist in certain Q ranges (for instance, Figs. 5 and 6). This new behavior is also a result of the formation of clusters for increasing system size. The possibility that one of the $IHLC$ distributions will overlap with the $IHSS$ from another cluster distribution (containing less elements in the lower level) increases significantly. Hence, we can state that the increase of the stability regions of the inhomogeneous states ($IHSS$ and $IHLC$) unraveled by the numerical simulations (Fig. 3) is a result of the cluster formation for growing populations, as we have determined from the bifurcation analysis presented.

Interestingly, the population displays even more complicated behavior when analysing the clustering effect in the $IHLC$ regime. This complexity is manifested through the formation of sub-clusters in the lower (oscillatory)

state, where oscillators exhibit identical behavior within a single sub-cluster, but with various phase relations among them. The simplest case consists of only two oscillators located on the lower oscillatory level – they are organized in anti-phase. However, increasing the number of oscillators in the lower state reveals multitude of relations between the oscillators grouped in sub-clusters and hence, besides the distribution of oscillators between the upper and lower states, one needs to consider also the composition of the oscillatory sub-clusters in the lower protein level. Figures 7 to 9 illustrate some examples of possible combinations of partitions and phase relations in the sub-threshold oscillations for an ensemble of $N = 18$ oscillators which we discuss next.

Due to the technical difficulty to handle a high-dimensional system with the *Xppaut* package, we present here only numerical findings. Please note the non-uniform distribution of the phase in some situations. The basic distribution of IHLC can be seen in Fig. 7(left), with only one element in the lower state. However, if an additional element is located in the lower state as well, (Fig. 7, middle), the phase-repulsive cell-to-cell communication evokes anti-phase oscillations, as already mentioned. In the situation where three cells are located in the lower state, stable out-of-phase oscillations with a phase-shift of $\frac{2\pi}{3}$ between clusters (Fig. 7, right) are observed, since the phase-repulsive coupling maximizes their phase difference.

Additional oscillators in the lower state contribute to the formation of more complex distributions. A fourth cell expressing a low *CI* protein concentration can establish a separate sub-cluster, which leads to the regime $(1:1:1:1)L \mid 14U$ (each sub-cluster is composed of isolated cells, as shown in Figs. 8, left and middle) or to a sub-cluster with more than one cell (e.g.

two sub-clusters are formed, each containing two cells, as in Fig. 9 middle). It is interesting to note, that the regime $(1:1:1:1)L \mid 14U$ has two realizations with different phase relations between the self-oscillatory cells in the low *CI* level. The left panel of Fig. 8 shows a nearly equal spaced phase shift of about $\frac{2\pi}{4}$, while the middle panel shows the case of an inhomogeneous phase shift. In particular, the cells are observed to come close to each other (two of them), but they never merge to form a sub-cluster. The right panel in Fig. 8 shows a more complex phase relation in which 5 out of the 18 cells are in the low-protein state, oscillating separately with an inhomogeneous phase-difference. This phase-regime is similar to the one in the middle plot of Fig. 8, but with an additional oscillator in between the other four clusters. The corresponding six time series given in Figs. 7–8 correspond to the same parameter values, for $N = 18$ and a fixed coupling value $Q = 0.2$. Thus the different dynamical behavior observed here originates only from different initial conditions.

It is important to note once again that a particular cluster distribution is characterized with a distinct level of protein concentration expressed in the cell. Namely, larger number of oscillators in the lower state reduces the protein concentration in the higher state. Moreover, we have also observed that the ratio ($r = \frac{N-m}{m}$) of the number of oscillators in both levels affects the amplitude of the limit cycle oscillations located in the lower protein level: $r < 1$ results in increased amplitude values. Additionally, the ratio r contributes to the changes in the period of oscillation, having as a consequence a well pronounced multirhythmicity in the system. Table 1 lists the observed periods and phase relations for the different ratios in the cases discussed in

Figs. 7–8. In the present case of $N = 18$ and $Q = 0.2$, every additional oscillator in the lower CI level of the IHLC lengthens the period by ≈ 1.2 time units, which leads to a significant change in the period between different distributions. A modification of the phase relation by a fixed partition ratio does not influence the period (left and middle panels of Fig. 8).

Due to the dynamical complexity of the system, which as mentioned above is a direct consequence of the clustering, it is useful to look into the stability of the different regimes (HSS, $IHSS$, $IHLC$), in order to define a general prediction scheme to determine which solution is dominant under different conditions. We have therefore calculated 1000 time series for a growing population size N, with different random initial conditions for every parameter set, using the approach discussed in Sec. 2. These initial conditions cover the $7N$-dimensional phase space of the system (7 degrees of freedom per oscillator) densely enough such that one can detect stable coexisting attractors with a significant basin of attraction. Figure 10 shows in detail the system size effect for two specific coupling values, ($Q = 0.24$ and $Q = 0.3$). In both cases, the results show a clearly monotonic increase of the probability that the $IHSS$ is reached from random initial conditions at the expense of the HSS, as the size of the population grows. For ensembles larger than several hundred cells the $IHSS$ is the dominant region, allowing us to speculate that the artificial differentiation of cells is strongly dependent on the size of the population, becoming more likely with proliferation (Koseska et al. (2009)). In other words, the stable inhomogeneous steady state resembles Turing's dissipative structure (Turing (1952)), only without space variables. In a sense, instead of the spatial Turing structure, in $IHSS$ we have a two cluster

decomposition present. This state, as discussed above, is characterized by two different stable protein concentration levels, which might be biologically interpreted as dynamical differentiation. Thus, one can further speculate that a robust dynamical differentiation of the cells strongly depends on the size of the population.

4. Full-amplitude oscillatory regimes - Regular and chaotic attractors

For couplings smaller than a given critical value $Q_{\mathrm{crit}} \sim 0.129$ (the value of Q_{crit} slightly varies depending on N), the system can only exhibit self-oscillatory solutions: we have identified out-of-phase oscillations with a number of different phase-shifts (e.g. $\frac{\pi}{2}$, $\frac{3\pi}{4}$, etc.). In contrast to the $IHLC$ solution, the attractors here share the same phase space. These full-amplitude oscillatory regimes, as we will further denote them, are dynamically very rich, displaying a diversity of sub-regimes for increasing coupling values. In particular, similarly to the minimal system of $N = 2$, we found two main types of behavior depending on the coupling strength Q:

- regular oscillations with stable cluster formation;
- chaotic self-oscillations with only a temporary cluster formation (we will denote this as grouping in the following discussion).

In what follows, we investigate the general characteristics of these regimes by means of bifurcation and numerical analysis. However, in order to distinguish between separate cluster formations for increasing population sizes via numerical simulations, we use the following definition: oscillators i and

j belong to the same cluster K at time t if the difference between the internal AI concentrations $S_i(t)$ and $S_j(t)$ at consecutive sampling time events is smaller than a pre-defined value $\varepsilon = 0.001$:

$$\begin{aligned} &[\mathrm{osc}_i(t), \mathrm{osc}_j(t)] \in \mathrm{clust}_K(t) \\ &\text{if } |S_i(t) - S_j(t)| \leq \varepsilon \text{ and} \\ &|S_i(t - \Delta t) - S_j(t - \Delta t)| \leq \varepsilon \ . \end{aligned} \tag{10}$$

The cluster sampling occurs every $\Delta t = 64$ time units, which is larger than the average period of the oscillations (the average period of oscillations is between 40 and 50 time units or approx. 200 min). Using these criteria, we classify the clustering of the oscillators, and present the resulting structures in the form of cluster plots (Figs. 12, 13, 15, 16), where the x-axes denote time, and the y-axes represent the oscillator index. There, we use different colors to encode the cluster number to which each element belongs (white color represents a free-running oscillator, which does not belong to any of the clusters). Although these plots do not show the dynamics of the self-oscillations in detail, they focus on the difference in the protein concentrations of separate cells over time, and therefore enable a visualization of the long-time cluster dynamics.

4.1. Regular attractors

Under small and intermediate couplings ($0 \leq Q \lesssim 0.55$), the system demonstrates regular oscillations with a fixed unique amplitude and common period for all oscillators (Fig. 12, top panel). In this case, the repulsive cell-to-cell communication evokes the preference of phase-shifted oscillations,

and small ensembles with $N \leq 4$ show solutions without clustering and homogeneously distributed phases (Fig. 2c). The phase shift here depends on the size of the system, and obeys the relation $\frac{2\pi}{N}$ (a solution known also as a "splay-phase" solution (Kaneko (1991); Watanabe and Strogatz (1993); Nicolis and Wiesenfeld (1992))). Hence, in a system of three coupled repressilators, one can find stable full-amplitude oscillations phase-shifted by $\frac{2\pi}{3}$ between HB_1 ($Q = 1.253$) and TR_1 (torus bifurcation for $Q = 1.11$), and from $Q = 0$ until $TR_2 = 0.55$ (see Fig. 11). No other stable cluster decomposition was identified from the bifurcation analysis. For $Q < 0.129$, and as mentioned above, this is the only stable solution of the system, whereas for increasing coupling the full-amplitude regime coexists with HSS, IHSS, and IHLC states, as shown in Fig. 11.

In systems where $N > 5$, clustering is observed in the regular oscillatory regime. Here, the 3-cluster decomposition dominates, with a nearly equal number of oscillators in each one (for details see Table 2), and a distinct phase relation between separate clusters. Morever, the periods of oscillation are slightly shorter than those of isolated elements, and decrease as Q increases (Table 2). We show here an example of a system of $N = 18$ cells. The onset of clustering can be seen in the cluster plot in the bottom panel of Fig. 12. After a long transient (about 1.200 time units, in this particular case) a distribution of three clusters is stabilized, with a $7 : 6 : 5$ distribution of oscillators (cells) between the clusters, and a phase shift of about $\sim \frac{2\pi}{3}$ among them. Time series of the separate clusters (the oscillators within each cluster display synchronous behavior) are given in the top panel of Fig. 12 (the coloring coresponds to the cluster plot). The long transient in

the simulation looks unphysiological at first glance, but all simulations are drawn from random initial conditions with a very large diversity amongst the cells. We use those unrealistic initial conditions in order to underline the ability of the system to form stable clusters under any condition. After proliferation, the daughter cells are in a similar phase as the mother, which decreases the formation of stable clusters significantly.

In the cases investigated, all the oscillators are identical and coupled via a mean field, hence there are no preferences amongst them to establish a given set of clusters. Thus the distribution of the oscillators between the clusters depends exclusively on the initial conditions. Several typical attractors observed for different system sizes and coupling values Q are listed in Table 2, together with the values of their periods. As shown here, the 3-cluster decomposition with nearly equal distribution of oscillators between the clusters dominates for large system sizes and over wide ranges of coupling. An exception to this case, as discussed above, is the formation of clusters for $N \leq 4$. In the case for $N = 4$, for instance, the 3-cluster decompositions lose stability, and stable 4-cluster decompositions are formed. Interestingly, the coupling Q has an inverse influence on the oscillation period. Normally, stronger coupling lengthens the period of coupled systems (Crowley and Epstein (1989); Volkov and Stolyarov (1994)), but the situation is different in the present case because Q controls the reinflux of AI and a higher internal AI concentration shortens the repressilator cycle. Compared to the coupling strength Q, the system size N and the cluster composition have a minor influence on the period.

4.2. Influence of parameter heterogeneity on the regular-attractor regime

The previous investigations analyzed in detail the dynamics of the regular attractors, as a first step in the understanding of the global cooperative behavior of large populations. However, the assumption that the elements of the system are identical (differing only in the initial conditions) is very strong, since cellular populations are heterogenous. It is therefore important to account for diversity among parameter values in separate cells by introducing, for e.g. certain missmatch in the α parameter values. In particular, we consider here that for each cell $i = 1, \ldots, 11$ different α's are assigned from a defined set of values $[210, 211, \ldots, 220]$, which leads to variability larger than 3% in the oscillation periods. Introducing the diversity exactly in α is realistic, since this parameter defines the expression strength of the repressilator genes, which is proportional to the concentration of repressilator plasmids present in the cell. The control of the number of plasmid copies in experiments was discussed in (Paulsson and Ehrenberg (2001)), and it can be coordinated with the cell's growth and division. Additionally, an increase in α lengthens the period of oscillations, as already mentioned.

We have observed that even in the presence of diversity, the three-cluster decomposition is the most probable state in the system (an example for $Q = 0.5$ is given in Fig. 13). However, in contrast to the case of identical oscillators, some of the cells (in the case of Fig. 13, the two elements with the smallest parameter α, i.e. the cells with the shortest period), are not phase locked and jump periodically from one of the three stable clusters to the other one. Moreover, the heterogeneity introduced via the parameter mismatch breaks the symmetry present in the system of identical oscillators,

and leads to a situation where oscillators with similar properties (i.e. similar α_i) group together in a cluster, preferentially.

4.3. Irregular self-oscillations

The bifurcation analysis we have performed on the model for $N = 3$ cells shows that for $Q \gtrsim 0.55$, the system goes beyond the range of regular oscillations: the periodic branch loses its stability between two torus bifurcations (TR_1 and TR_2 in Fig. 11), which contributes to the appearance of oscillations with strong variations of the amplitude. These irregular oscillations look very similar to chaotic time series (Fig. 15, top plot), however, in order to classify this as a chaotic behavior, certain criteria need to be fullfilled, e.g. at least one of the Lyapunov exponents of the system needs to be positive. Therefore, we integrate forward in time a small perturbation of the trajectory, the random tangent vector, by means of the Jacobi matrix. The logarithm of the norm of the tangent vector is related to the maximal Lyapunov exponent (Eckmann and Ruelle (1985)) and we normalize it by the integration time. The result is plotted in the top panel of Fig. 14, and shows that for $Q > Q_{chaos} \approx 0.6$ (upper boundary of $Q \approx 1$), clear chaotic behavior with a positive maximal Lyapunov exponent is observed. The bottom panel of Fig. 14 displays a bifurcation diagram computed as a series of Poincaré sections, with the ordinate showing the value of the B_1 when the trajectory crosses $A_1 = 4.0$. We avoid the tracking and evaluation of unstable attractors and numerical artifacts by adding small dynamical noise to the transcription dynamics of the *tetR* $mRNA$, i.e. we add the term $\xi_i(t)$ to the rhs of Eq. 1. The local noise term $\xi_i(t)$ is assumed to be Gaussian, with zero mean and intensity σ_a^2 defined by the correlation $\langle \xi_i(t)\xi_j(t+\tau)\rangle = \sigma_a^2 \delta(\tau)\delta_{i,j}$. Beside

being technically useful, the noise is biologically relevant, as it is caused by random fluctuations in transcription due to the small number of involved $mRNA$ (Elowitz and Leibler (2000)).

In contrast to the case of the minimal system ($N = 2$), where a similar irregular dynamic with chaotic behavior was observed (Ullner et al. (2008)), the extended system studied here ($N = 18$ in Fig. 14) is characterized by the ability to build temporal clusters, which we refer to as grouping. The coupling Q changes the chaotic behavior gradually (top panel in Fig. 14). A first weak increase of the maximal Lyapunov exponent is followed by a fast rising interrupted by short collapse and a final decline to zero at $Q \approx 1$. The degree of chaos influences the grouping ability, as chaos destabilizes and shortens the grouping. In the parameter range of Q where more irregular than simple periodic oscillations are observed, $0.55 \lesssim Q$, temporal $2-$, $3-$, $4-$ or $5-$ grouping decompositions with a significant lifetime have been observed, in contrast to the regular attractors, where the $3-$cluster decompositions were the dominant ones.

The example in Fig. 15 shows a weak chaotic dynamics of $N = 18$ oscillators at $Q = 0.6$, with long-living 3- and 4-grouping constellations. The cluster plot (bottom panel of the figure) illustrates the interplay of long-time grouping and recurring transients with less ordered states, while a rearrangement to a new grouping happens. The groupings are long living up to $20,000$ time units, i.e. about 4000 cycles. Due to the symmetry of the system in the case of identical elements, separate oscillators do not have local grouping preferences. The bottom plot of Fig. 15 gives a detailed insight on the oscillatory dynamics at different times, and shows the long-living 3- and 4-

grouping constellations, and transients with a high degree of decomposition. However, once the oscillators are distributed in a long-living grouping state, they oscillate synchronously within the group and cannot be distinguished by their time series until the next decomposition occurs and spreads the phases.

The second example of irregular chaotic self-oscillations (Fig. 16) illustrates a regime of fully developed chaos at high coupling $Q = 0.75$. The maximal Lyapunov exponent (Fig. 14) increases significantly above zero, which confirms the chaotic character of the dynamics. Interestingly, the temporal grouping of the oscillators is conserved, but with a significantly shorter lifetime and faster mixing as compared to the weak chaotic dynamics discussed above (Fig. 15). Despite the fact that clusters are not stable in this parameter range, some of the oscillators run in-phase over long time and fulfill the clustering condition (Eq. 10) temporarily. In this typical situation shown here for fully developed chaos at $Q = 0.75$ (Fig. 16) the grouping of the oscillators can last over a relatively long time and cover up to $5,000$ time units, i.e. more than 100 oscillations. The individual repressilators oscillate in an irregular manner with fluctuating amplitude and period. The top panels of Fig. 16 shows different snapshots of the time series, and the bottom panel of the figure shows the corresponding cluster plot and illustrates the interplay between grouping and decomposition. Note the larger maximal amplitudes in the more ordered case than in the situation where higher degree of decomposition is observed.

In general, it can be stated that inside the chaotic ensemble there exists an everlasting tendency to build and break temporal groups, which leads to their mixing. Many different temporal distributions of the oscillators into

groups are possible, which survive over several oscillation periods until the next mixing occurs. In the case investigated here in detail, $N = 18$ oscillators, we have observed e.g. two temporal groups with a distribution $9 : 9$ of the oscillators between them, three groups with distributions $7 : 6 : 5$, and $7 : 7 : 4$, four temporal groups with distributions $8 : 6 : 3 : 1$, $7 : 6 : 4 : 1$, $5 : 5 : 5 : 3$, and $5 : 5 : 4 : 4$, as well as several examples of five groupings decompositions, with distributions such as $6 : 5 : 4 : 2 : 1$, $5 : 5 : 4 : 2 : 2$, $5 : 5 : 4 : 3 : 1$ or $5 : 4 : 4 : 3 : 2$. Several other examples with a higher degree of decomposition can be observed as well, however, they exhibit a much shorter lifetime. The observed clustering effects resemble the dynamical behavior of globaly coupled maps reported by Kaneko in (Kaneko (1990)). The transition from an ordered to a partially ordered and turbulent phase, where the number of clusters is significantly increased is similar to the case of a weak and well developed chaotic clustering decomposition ordering, discussed in this section. Moreover, we show that a growing system size increases the possibility for grouping formation significantly, as well as the number of different distributions of the oscillators between the groups, which on the other hand enhances the flexibility of the system. This means that by varying environmental conditions, the population can switch between different distributions to adapt to its surroundings and improve its fitness. Although the chaotic dynamics observed here and the effect of intrinsic noise in synthetic oscillators (Elowitz and Leibler (2000); Stricker et al. (2008)) have very similar manifestations despite their different origins, we intend to draw the readers' attention to chaos as an alternative source of uncertainty in genetic networks.

The chaotic dynamics and the grouping phenomena appear graduately for increasing coupling Q, i.e. at cell densities which could be a cause for stress. One could speculate, that the population has the flexibility to respond to environmental stress by distributing its cells within stable clusters, and thus increasing the variability and diversity amongst the different cells to enhance the probability to survive the stress situation. The gradual chaotic behavior enables the population to adapt the mixing velocity and the degree of diversity to the stress conditions.

5. Discussion

The mechanism how a multicellular system assures a robust and coordinated response in a noisy and fluctuating environment is still an intriguing question. It has been suggested however, that the intercellular signaling plays one of the crucial roles in the establishment of cooperative functioning in populations. In that contex, we attempt here to characterize the dynamical behavior of multicellular systems using phase-repulsively coupled synthetic genetic repressilators [Eqs. (1)–(7)]. The focus in the current paper is on the dynamics of large and growing ensembles, but we also compare our results with the recent findings on the basic ensemble of two coupled repressilators, by means of numerical simulations of the dynamics and bifurcation analysis.

We show that a multicellular population of synthetic genetic repressilators displays various dynamical behavior, e.g. full-amplitude self-oscillations, homogeneous steady state (HSS), inhomogeneous steady state ($IHSS$), and inhomogeneous limit cycle ($IHLC$). These regimes are present for all population sizes, and may in general coexist with each other. Moreover, the size of

the system affects the relative sizes of the basins of attraction of each regime. For instance, the inhomogeneous states become more likely for larger populations. Interestingly, those inhomogeneous regimes can be associated with permanent artificial cell differentiation in synthetic genetic networks, and the simulations predict that a growing system size, e.g. due to proliferation, enhances the probability of differentiation. Additionally, large system sizes widen the parameter range of the $IHLC$ and $IHSS$ regimes significantly, and further enhance the differentiation probability.

Furthermore, the understanding of cell differentiation (Kaneko and Yomo (1997); Furusawa and Kaneko (2001)) and its connection to the emergence of stable attractors from cell-to-cell coupling is still not clear. Here, we have investigated systematically the mechanisms through which coexisting attractors arise in the multicellular system. Namely, a closer look into the inhomogeneous regimes ($IHLC$ and $IHSS$) shows a splitting of the single attractor that exists for two coupled elements into multiple coexisting solutions for many oscillators, and the number of stable attractors increases with the system size. A combination of numerical simulations and bifurcation analysis revealed that the different stable $IHSS$ solution branches differ by the number of elements in the high and low protein levels, and that each distribution implies a new attractor with different stability ranges and individual protein levels. The $IHLC$ is on the other hand, directly bounded to the $IHSS$ with the same distribution of the oscillators via a Hopf bifurcation. The ability of the $IHLC$ regime to build oscillating clusters with different phase relations in the low protein level increases further the number of sub-regimes, and includes multi-rhythmicity as a tunable clock (similarly to the tunability of the

$IHSS$ regimes) because the attractors express different typical frequencies. One can further speculate that this feature can be seen as an example of the adaptability of a population to easily adjust its cell distribution when environmental changes occur, in order to respond and adapt optimaly to the surrounding.

Similar behavior was observed in the full-amplitude self-oscillatory regime: various oscillatory clusters with different partitions of the oscillators amongst them. Moreover, the spectra of possible constellations increases with the system size. For small and intermediate coupling Q, stable self-oscillations characterized with a 3-cluster decomposition, and phase shifted by $\sim \frac{2\pi}{3}$ appear. These 3-cluster decompositions are very robust to perturbations, in the form of e.g. random initial conditions, dynamical noise or parameter heterogeneity. The direct numerical investigations performed here can not guarantee the "mathematical" stability of the discussed clustering regimes. However, taking in mind recent results (Ashwin et al. (2007)) we can suggest that these clusters belong to a heteroclinic network and demonstrate switching which is manifested more effectively in the presence of detuning. This question itself deserves further attention but in any case, the regimes observed here have very long life times which certainly makes them interesting and important for biology.

Furthermore, an increasing cell density caused by cell growth and proliferation increases effectively the coupling Q, and up to a critical coupling $Q_{\text{crit}} \approx 0.6$ the regular self-oscillations become unstable, turning into chaotic oscillations with high variability in their amplitude and frequency. Interestingly, also in the presence of chaos the population tends to build temporal

clusters, which we refer to as groups. These temporal groups of co-jointly oscillating repressilators have a significant lifetime, depending on the degree of chaos, and are interrupted by recurring decomposition of the groups and a reassembling into different groups. The chaotic dynamics appears gradually with Q, and allows the population to respond flexibly and sensitively to increasing stress via a higher dynamical diversity inside the ensemble.

In summary, our results show that a population of synthetic genetic clocks coupled via the mean field exhibit a significantly enhanced range of possible dynamical regimes with very different properties. One could speculate that the observed multi-stability and multi-rhythmicity, which increase with the system size, enhance the fitness of the cellular population under environmental stress, and optimize the adaptation of the colony by a sensitive adjustment of the protein dynamics.

6. Acknowledgments

A.K. and J.K. acknowledge the GoFORSYS project funded by the Federal Ministry of Education and Research, Grant Nr. 0313924, E.U. acknowledges financial support from SULSA, Deutsche Forschungsgemeinschaft (SFB 618) and the Alexander von Humboldt Foundation, E.V. the Program "Radiofizika" Russian Academy and RFBR Grant No. 08-0200682, 08-0100131, J.G.O. the Ministerio de Ciencia e Innovacion (Spain) (project FIS2009-13360 and I3 program) and J.K. the EU through the Network of Excellence BioSim, Contract No. LSHB-CT-2004-005137. This work has also been supported by the European Commission (project GABA, FP6-NEST contract 043309).

References

Ashwin, P., Orosz, G., Wordsworth, J., Townley, S., 2007. Dynamics on networks of cluster states for globally coupled phase oscillators. SIAM J. Appl. Dyn. Syst. 6, 728–758.

Balagadde, F. K., Song, H., Collins, C. H., Barnet, M., Arnold, F. H., Quake, S. R., You, L., 2008. A synthetic escherichia coli predator-prey ecosystem. Mol. Sys. Bio. 4:187, 1–8.

Crowley, M. F., Epstein, I. R., 1989. Experimental and theoretical studies of a coupled chemical oscillator: phase death, multistability and in-phase and out-of-phase entrainment. J. Phys. Chem. 93, 2496–2502.

Eckmann, J. P., Ruelle, D., 1985. Ergodic theory of chaos and strange attractors. Rev. Mod. Phys. 57 (3), 617–656.

Elowitz, M., Leibler, S., 2000. A synthetic oscillatory network of transcriptional regulators. Nature 403, 335–338.

Ermentrout, B., 2002. Simulating, Analyzing, and Animating Dynamical Systems: A Guide to Xppaut for Researchers and Students (Software, Environments, Tools). SIAM Press.

Furusawa, C., Kaneko, K., 2001. Theory of robustness of irreversible differentiation in a stem cell system: chaos hypothesis. J. theor. Biol. 209, 395–416.

García-Ojalvo, J., Elowitz, M. B., Strogatz, S. H., 2004. Modeling a synthetic

multicellular clock: Repressilators coupled by quorum sensing. Proc. Natl. Acad. Sci. U.S.A. 101 (30), 10955–10960.

Golomb, D., Hansel, D., Shraiman, B., Sompolinsky, H., 1992. Clustering in globally coupled phase oscillators. Phys. Rev. A 45, 3516–3530.

Heinlein, M., 2002. Plasmodesmata: dynamic regulation and role in macromolecular cell-to-cell signaling. Curr. Opin. Plant Biol. 5, 543–552.

Kaneko, K., 1990. Clustering, coding, switching, hierarchical ordering, and control in a network of chaotic elements. Physica D 41, 137–172.

Kaneko, K., 1991. Globally coupled circle maps. Physica D 54, 5–19.

Kaneko, K., Yomo, T., 1994. Cell division, differentiation and dynamic clustering. Physica D 75, 89–102.

Kaneko, K., Yomo, T., 1997. Isologous diversification: A theory of cell differentiation. Bull Math Biol. 59, 139–196.

Kiss, I. Z., Hudson, J. L., 2003. Chaotic cluster itinerancy and hierarchical cluster trees in electrochemical experiments. Chaos 13, 999–1009.

Koseska, A., Volkov, E., Zaikin, A., Kurths, J., 2007. Inherent multistability in arrays of autoinducer coupled genetic oscillators. Phys. Rev. E 75 (3), 031916(8).

Koseska, A., Zaikin, A., Kurths, J., García-Ojalvo, J., 2009. Timing cellular decision making under noise via cell–cell communication. PLoS ONE 4, e4872.

695 Kuznetsov, A., Kærn, M., Kopell, N., 2004. Synchrony in a population of
696 hysteresis-based genetic oscillators. SIAM Journal on Applied Mathematics
697 65 (2), 392–425.

698 Kuznetsov, A., Kurths, J., 2002. Stable heteroclinic cycles for ensembles of
699 chaotic oscillators. Phys. Rev. E 66, 026201.

700 Manruiba, S., Mikhailov, A., 1999. Mutual synchronization and clustering
701 in randomly coupled chaotic dynamical networks. Phys. Rev. E 60, 1579–
702 1589.

703 McMillen, D., Kopell, N., Hasty, J., Collins, J. J., 2002. Synchronizing genetic
704 relaxation oscillators by intercell signaling. Proc. Natl. Acad. Sci. U.S.A.
705 99 (2), 679–684.

706 Miyakawa, K., Yamada, K., 2001. Synchronization and clustering in globally
707 coupled salt-water oscillators. Physica D 151, 217–227.

708 Nakajima, A., Kaneko, K., 2008. Regulative differentiation as bifurcation of
709 interacting cell population. J Theor. Biol. 253(4), 779–787.

710 Nicolis, S., Wiesenfeld, K., 1992. Ubiquitous neutral stability of splay-phase
711 states. Phys. Rev. A 45, 8430–8435.

712 Okuda, K., 1993. Variety and generality of clustering in globally coupled
713 oscillators. Physica D 63, 424–436.

714 Osipov, G., Kurths, J., Zhou, C., 2007. Synchronization in oscillatory net-
715 works, 1st Edition. Springer, Berlin.

716 Paulsson, J., Ehrenberg, M., 2001. Noise in a minimal regulatory network:
717 plasmid copy number control. Q. Rev. Biophys. 34, 1–59.

718 Perbal, B., 2003. Communication is the key. Cell Commun. Signaling 1, 1–4.

719 Stricker, J., Cookson, S., Bennett, M. R., Mather, W. H., Tsimring, L. S.,
720 Hasty, J., 2008. A fast, robust and tunable synthetic gene oscillator. Nature
721 456, 516–519.

722 Taga, M. E., Bassler, B. L., 2003. Chemical communication among bacteria.
723 Proc. Natl. Acad. Sci. U.S.A. 100, 14549–14554.

724 Tanouchi, Y., Tu, D., Kim, J., You, L., 2008. Noise reduction by diffu-
725 sional dissipation in a minimal quorum sensing motif. PLoS Comp. Biol.
726 4, e1000167.

727 Turing, A., 1952. The chemical basis of morphogenesis. Phil. Trans. R. Soc.
728 Lond. B 237, 37–72.

729 Ullner, E., Koseska, A., Kurths, J., Volkov, E., Kantz, H., García-Ojalvo, J.,
730 2008. Multistability of synthetic genetic networks with repressive cell-to-
731 cell communication. Phys. Rev. E 78, 031904.

732 Ullner, E., Zaikin, A., Volkov, E. I., García-Ojalvo, J., 2007. Multistabil-
733 ity and clustering in a population of cellular genetic oscillators via phase
734 repulsive cell-to-cell communication. Phys. Rev. Lett. 99, 148103.

735 Volkov, E. I., Stolyarov, M. N., 1994. Temporal variability in a system of
736 coupled mitotic timers. Biol. Cybern. 71, 451–459.

737 Wang, W., Kiss, I. Z., Hudson, J. L., 2001. Clustering of arrays of chaotic
738 chemical oscillators by feedback and forcing. Phys. Rev. Lett. 86, 4954–
739 4957.

740 Watanabe, S., Strogatz, S. H., 1993. Integrability of globally coupled oscilla-
741 tor array. Phys. Rev. Lett. 70, 2391–2395.

742 You, L., Cox III, R. S., Weiss, R., Arnold, F. H., 2004. Programmed popula-
743 tion control by cell-cell communication and regulated killing. Nature 428,
744 868–871.

745 Zhou, T., Zhang, J., Yuan, Z., Chen, L., 2008. Synchronization of genetic
746 oscillators. Chaos 18, 037126.

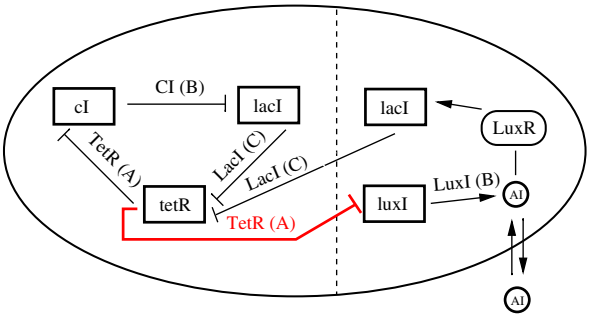

Figure 1:

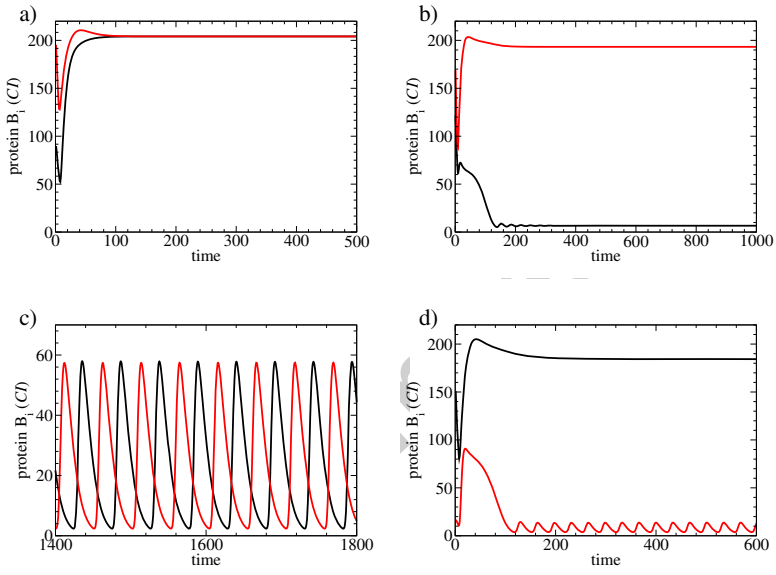

Figure 2:

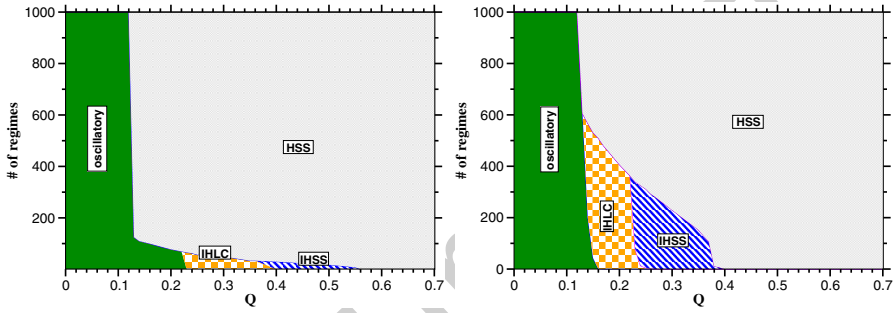

Figure 3:

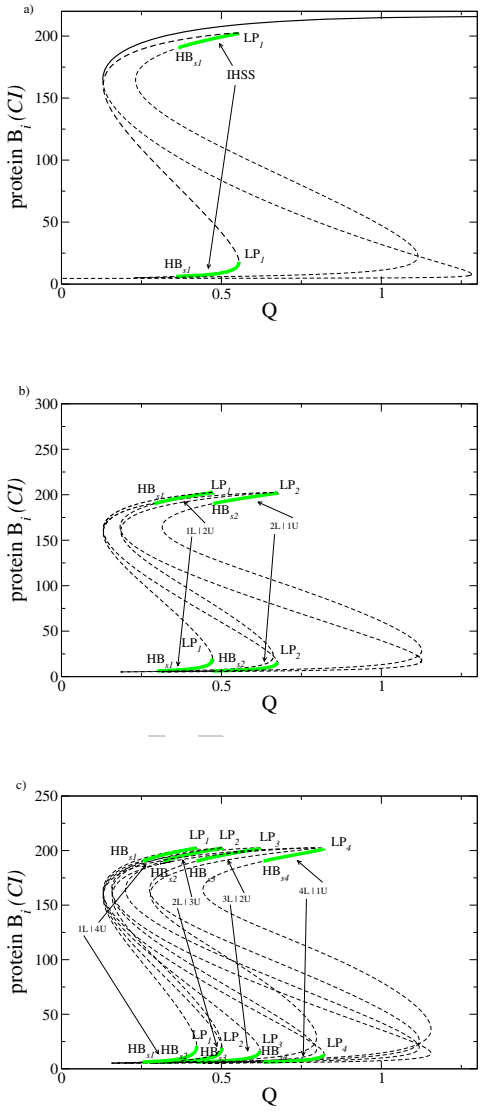

Figure 4:

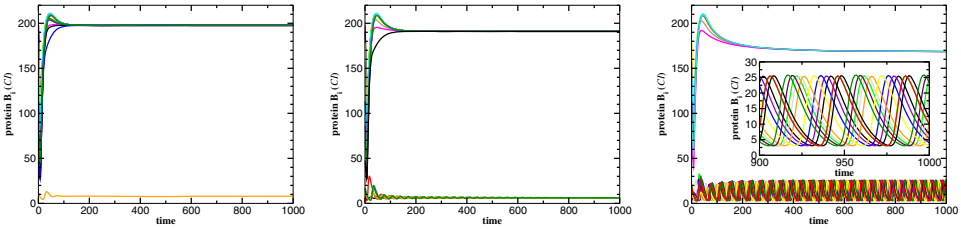

Figure 5:

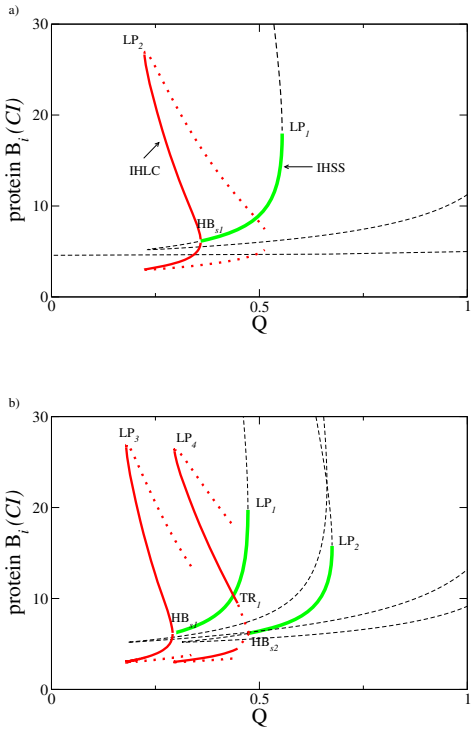

Figure 6:

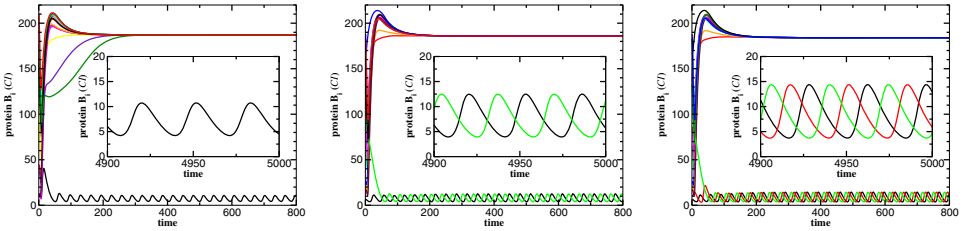

Figure 7:

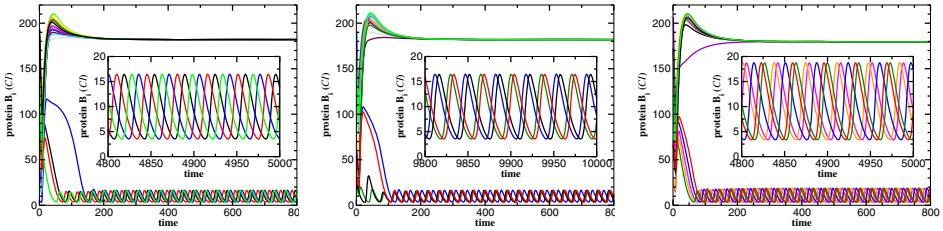

Figure 8:

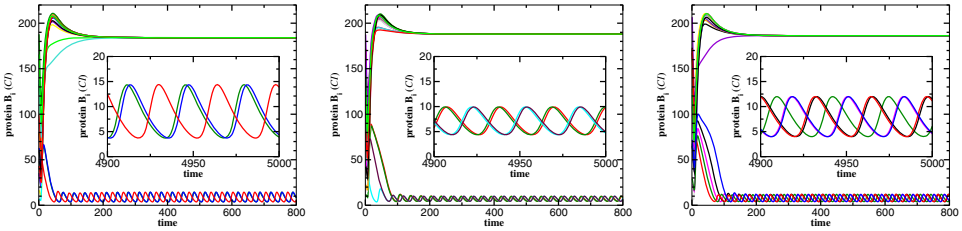

Figure 9:

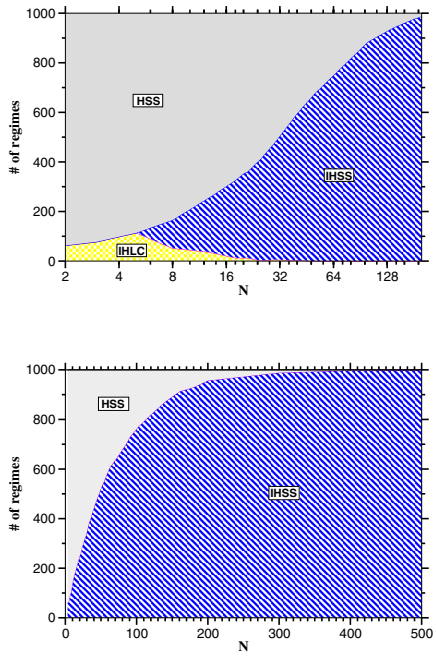

Figure 10:

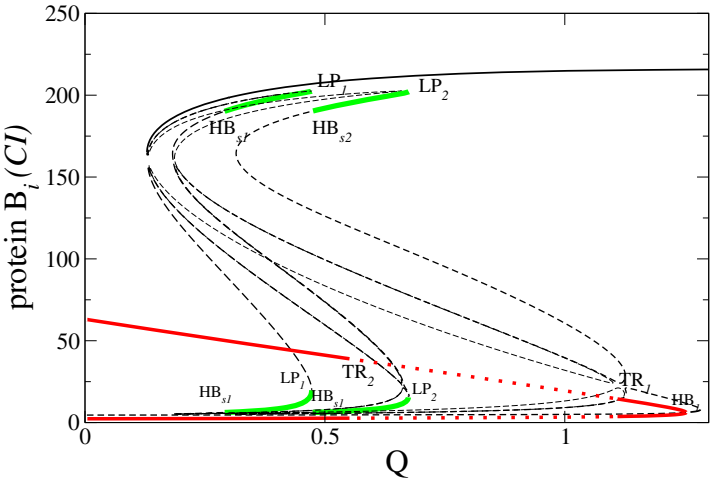

Figure 11:

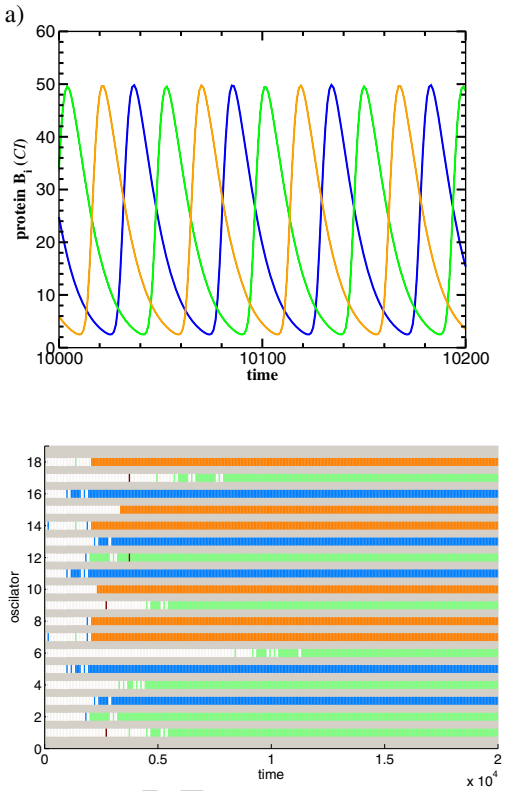

Figure 12:

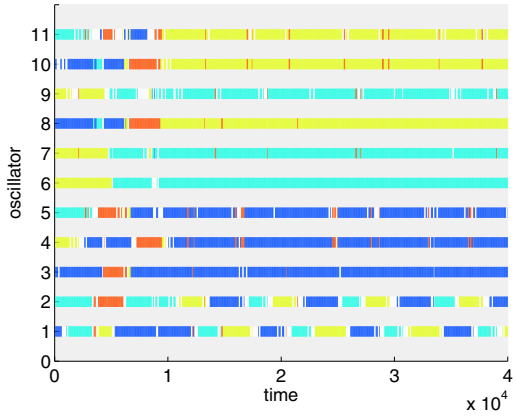

Figure 13:

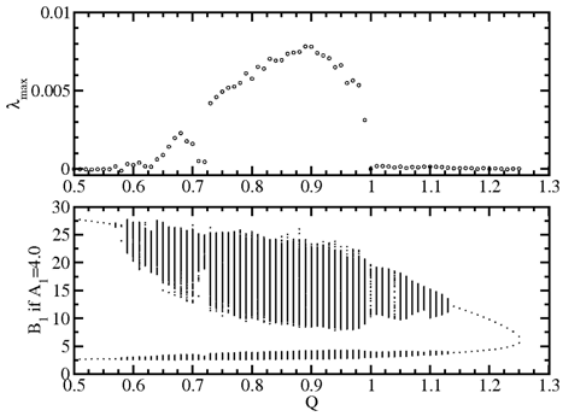

Figure 14:

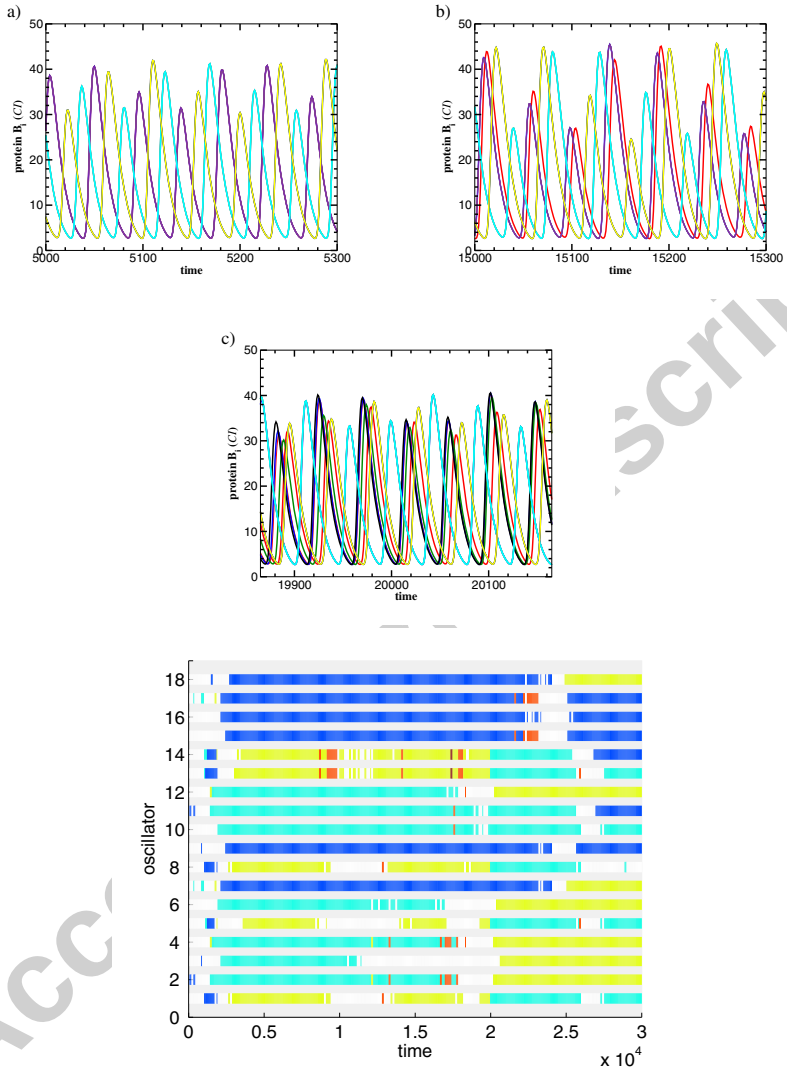

Figure 15:

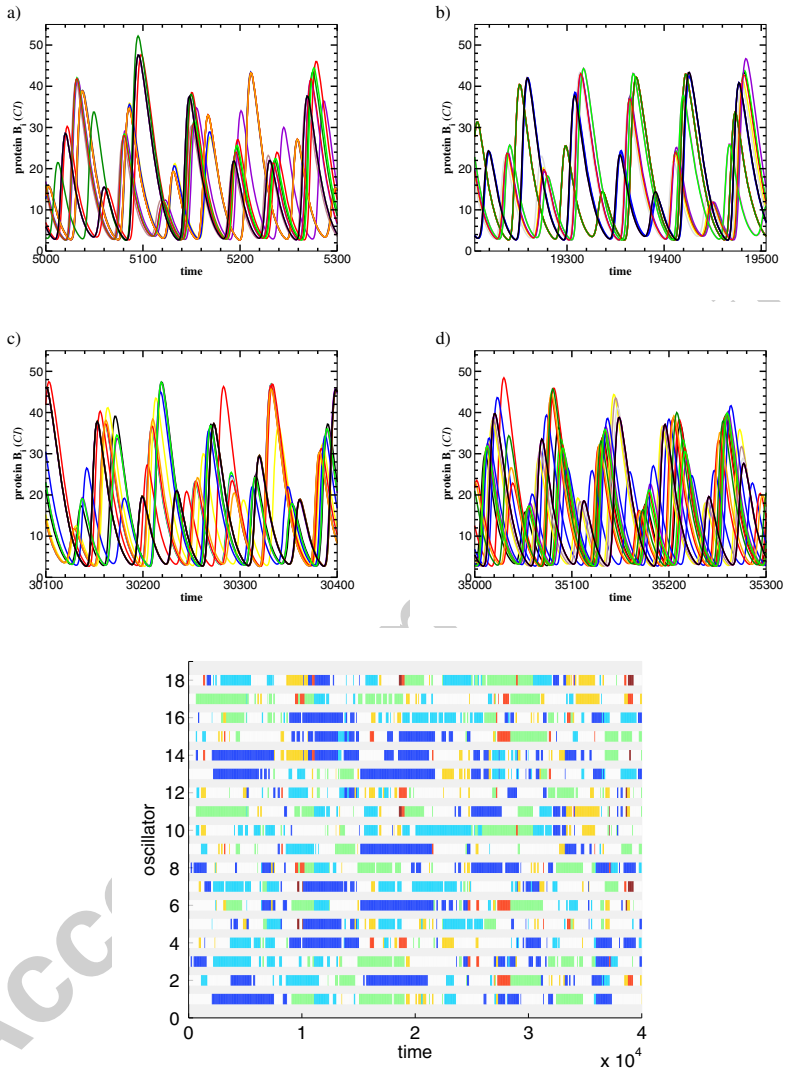

Figure 16:

Figure Legends

Figure 1.

Scheme of the repressilator with repulsive quorum sensing cell-to-cell communication.

Figure 2.

Time series for different dynamical regimes for the minimal coupled system of $N = 2$: a) $Q = 0.4$, homogeneous steady state; b) $Q = 0.4$, inhomogeneous steady state; c) $Q = 0.1$, full amplitude oscillations and d) $Q = 0.3$, inhomogeneous limit cycle. The other parameters are: $n = 2.6$, $\alpha = 216$, $\beta_a = 0.85$, $\beta_b = 0.1$, $\beta_c = 0.1$, $\kappa = 25$, $k_{s0} = 1.0$, $k_{s1} = 0.01$, $\eta = 2.0$.

Figure 3.

Influence of the system size ($N = 2$ in the left plot and $N = 18$ in the right plot) on the relative regime separation versus coupling strength Q. Other parameters as in Fig. 2.

Figure 4.

Bifurcation chart depicting stable IHSS for: (a) $N = 2$; (b) $N = 3$ and (c) $N = 5$ oscillators. Other parameters as in Fig. 2. Here, thick (green) solid lines denote stable $IHSS$ cluster decompositions, and dashed lines denote unstable steady state. Note that the bifurcation charts are not complete, depicting only those parts relevant for the current discussion.

Figure 5.

Time series of protein CI (B_i) for the IHSS in two different cluster distributions: $1L \mid U17$ (left plot) and $6L \mid 12U$ (middle plot) and an example of IHLC (right plot) coexisting for the same parameters, with fixed system size $N = 18$ and $Q = 0.3$. The IHLC example contains 6 oscillators in the upper CI state and 12 in the lower one.

Figure 6.

Bifurcation structure of the $IHLC$ regime for (a) $N = 2$, solid (red) line, and (b) $N = 3$ oscillators - the left solid (red) line denotes stable $1L \mid 2U$ distribution, whereas the right one denotes stable $2L \mid 1U$ distribution. Other parameters as in Fig. 2. Due to the large stiffness of our multidimensional model and the proximity to the bifurcation point, the correct continuation could not be performed with the *Xppaut* package. Therefore, the bifurcation branches on this figure are not closed.

Figure 7.

Examples of different IHLC distributions in an ensemble of $N = 18$ cells for the same coupling $Q = 0.2$. Every oscillatory sub-cluster consists of only one cell: $1L \mid 17U$ (left), $1 : 1L \mid 16U$ (middle), and $1 : 1 : 1L \mid 15U$ (right). The insets show a detail of the low-level oscillations after transients. Other parameters as in Fig. 2.

Figure 8.

$IHLC$ states exhibiting oscillatory low-protein-level sub-regimes with four (left and middle) and five (right) elements in an ensemble of $N = 18$ cells. Every sub-cluster in the oscillatory state consists of only one cell. Here $Q = 0.2$ and other parameters as in Fig. 2. The left figure depicts the situation with equal phase distance between the oscillating repressilators in the low protein B level, while in the middle and right plots the phase distances are different. The insets belong to the same time series and show a detail of the oscillatory sub-clusters.

Figure 9.

Examples of IHLC states with complex phase relations between the oscillatory sub-clusters in an ensemble of $N = 18$ cells. The insets show in detail the small limit cycle oscillations in the lower-protein state. Parameters are $Q = 0.2$ with $(2 : 1)L \mid 15U$ (left), $Q = 0.24$ with $(2 : 2)L \mid 14U$ (middle), $Q = 0.24$ with $(2 : 2 : 1)L \mid 13U$ (right). Other parameters as in Fig. 2.

Figure 10.

Distribution of dynamical regimes (HSS, IHSS, IHLC) for increasing cell numbers. The coupling strength is fixed to $Q = 0.24$ (top) and $Q = 0.3$ (bottom). Other parameters as in Fig. 2.

Figure 11.

Bifurcation diagram of 3 coupled repressilators for increasing Q, illustrating the stability of different steady-state and periodic

branches. Due to limitations of the *Xppaut* package to produce a complete bifurcation diagram of the system, we have used here a small diversity in the α parameter values of different oscillators in the range of 10^{-3}. This does not qualitatively change the results, but is a sufficient condition to obtain the complete bifurcation structure of the system. For convenience, we have plotted here only one of the oscillators, although the full analysis has been performed.

Figure 12.

Top: time series of the protein B_i concentration in the regular oscillating regime, exhibiting three cluster decompositions with $7:6:5$ distribution of cells between them. After a transient, a synchronous behavior inside each cluster emerges and the individual dynamics of the cells inside each cluster are indistinguishable. Bottom: cluster-plot representation of the case above. The parameters are those of Fig. 2, except $Q = 0.3$.

Figure 13.

Cluster plot of $N = 11$ non-identical repressilators in the self-oscillatory regime. A small diversity in parameter α_i makes the oscillators non-identical. α_i increases from bottom to top. The parameters are: $n = 2.6$, $\alpha_i = 210, 211 \ldots 219, 220$, $\beta_a = 0.85$, $\beta_b = 0.1$, $\beta_c = 0.1$, $\kappa = 25$, $k_{s0} = 1.0$, $k_{s1} = 0.01$, $\eta = 2.0$, and $Q = 0.5$.

Figure 14.

Maximal Lyapunov exponent (top) and a numerical bifurcation plot for the full amplitude oscillations (bottom) for increasing coupling Q. The simulations have small genetic noise $\sigma_a^2 = 10^{-8}$ to avoid tracking unstable orbits. $N = 18$, and other parameters are as in Fig. 2.

Figure 15.

Time series (top panels) and the corresponding cluster plots (bottom panel) in the self-oscillatory regime of $N = 18$ oscillators with weak chaotic behavior and long lasting grouping. Parameters are: $n = 2.6$, $\alpha = 216$, $\beta_a = 0.85$, $\beta_b = 0.1$, $\beta_c = 0.1$, $\kappa = 25$, $k_{s0} = 1.0$, $k_{s1} = 0.01$, $\eta = 2.0$, $\sigma_a^2 = 10^{-10}$, **and** $Q = 0.6$.

Figure 16.

Time series (top panels) and the corresponding cluster plot (bottom panel) in the self-oscillatory regime for $N = 18$ oscillators with strong chaotic dynamics and short-lived time grouping, for $N = 18$ repressilators. The parameters are: $n = 2.6$, $\alpha = 216$, $\beta_a = 0.85$, $\beta_b = 0.1$, $\beta_c = 0.1$, $\kappa = 25$, $k_{s0} = 1.0$, $k_{s1} = 0.01$, $\eta = 2.0$, $\sigma_a^2 = 10^{-10}$, **and** $Q = 0.75$.

Table 1: Examples of the dependence of the IHLC oscillation period on the oscillators distribution between the high- and low-protein levels for $N = 18$ and $Q = 0.2$.

# HIGH	# LOW	PHASE	FIGURE	PERIOD
17	1	-	7 left	≈ 31.7
16	2	equal	7 middle	≈ 32.9
15	3	equal	7 right	≈ 34.0
14	4	equal	8 left	≈ 35.3
14	4	complex	8 middle	≈ 35.3
13	5	complex	8 right	≈ 36.5

Table 2: Examples of the clustering of the full amplitude oscillations.

Q	cluster	phase	period
$N = 2$			
0.1	1:1	equal	51.3
0.15	1:1	equal	50.0
0.2	1:1	equal	49.4
0.3	1:1	equal	47.7
0.4	1:1	equal	46.0
0.5	1:1	equal	44.5
0.6	1:1	complex	*many*
$N = 3$			
0.1	1:1:1	equal	51.3
0.15	1:1:1	equal	50.7
0.2	1:1:1	equal	50.0
0.3	1:1:1	equal	48.8
0.4	1:1:1	equal	47.2
0.5	1:1:1	equal	46.1
0.6	1:1:1	complex	*many*

$N = 4$			
0.1	1:1:1:1	equal	51.3
0.15	1:1:1:1	equal	50.7
0.2	1:1:1:1	equal	50.1
0.3	1:1:1:1	equal	48.8
0.4	1:1:1:1	equal	47.6
	2:2	unstable	-
0.5	1:1:1:1	equal	46.0
	2:1:1	asymmetric	45.0
0.6	2:2	complex	*many*
$N = 5$			
0.0	-	-	52.7
0.15	2:2:1	equal	50.7
0.2	2:2:1	equal	50.0
0.3	2:2:1	equal	48.6
0.4	2:2:1	equal	47.2
0.5	2:2:1	equal	45.5
	3:2	unstable	-
0.6	2:2:1	equal	44.1

$N = 6$			
0.2	2:2:2	equal	50.1
	3:3	unstable	-
0.3	2:2:2	equal	48.4
0.4	2:2:2	equal	47.3
$N = 18$			
0.2	6:6:6	equal	50.0
	7:6:5	equal	50.0
	8:5:5	equal	50.0
	7:7:4	unstable	-
	8:6:4	unstable	-
	9:9	unstable	-
$N = 100$			
0.4	34:34:32	equal	47.2
	35:33:32	equal	47.2
	35:34:31	equal	47.2
	36:33:31	equal	47.1